Available online at www.sciencedirect.com
SCIENCE DIRECT®
Journal of Organometallic Chemistry 681 (2003) 196–209
Journal of Organometallic Chemistry
www.elsevier.com/locate/jorganchem

Synthesis, characterization, structure and luminescence studies of mono-, di- and trinuclear gold(I) phosphine alkynyl complexes

Vivian Wing-Wah Yam *, Kai-Leung Cheung, Sung-Kong Yip, Kung-Kai Cheung

Centre for Carbon-Rich Molecular and Nano-Scale Metal-Based Materials Research, Department of Chemistry and HKU-CAS Joint Laboratory on New Materials, The University of Hong Kong, Pokfulam Road, Hong Kong SAR, China

Received 16 May 2003; received in revised form 27 June 2003; accepted 27 June 2003

Abstract

A series of luminescent gold(I) phosphine mono- and diynyl complexes with nuclearity ranging from one to three has been synthesized and characterized; one of them have its crystal structure determined. Their photophysical properties have been studied and emission origin elucidated.

Keywords: Gold(I); Alkynyl ligands; Luminescence; Phosphine ligands

1. Introduction

Acetylenic compounds, especially terminal alkynes, are valuable synthetic intermediates and there have been enormous interests in the development of methods for introducing an ethynyl group into both organic and inorganic structures [1,2]. The linear geometry of the alkynyl unit together with its π-unsaturated nature have made the rigid metal alkynyl moieties ideal building blocks for the construction of molecular wires and organometallic oligomeric and polymeric materials that may possess unique properties such as optical nonlinearity, electrical conductivity, and liquid crystallinity [1–4].

During the last decade, the synthesis, molecular structures and chemistry of gold(I) phosphine alkynyl complexes have attracted growing attention, in part due to the reports on their rich luminescence properties [5,6] and their ability to build supramolecular structures [7] based on the aurophilic nature of gold. Herein are reported the synthesis, structure, electronic absorption, and luminescence properties of a series of mononuclear, dinuclear and trinuclear gold(I) phosphine complexes of mono- and diynyl ligands.

2. Experimental

2.1. Materials

Phenylacetylene (Aldrich), 2-methylbut-1-en-3-yne (Lancaster), pent-1-yne (Maybridge) and oct-1-yne (Maybridge) were used as-received. Bis[di(4-methylphenyl)phosphino]methane (dtpm) [8], 1,3-heptadiyne [9], 1,3-decadiyne [10], phenylbutadiyne [11], 2-ethynylthiophene [12], 5-ethynyl-2,2′-bithienyl [13] and the chlorogold(I) phosphine precursor complexes [14] were prepared according to literature procedures.

Dichloromethane (Lab Scan, AR) and tetrahydrofuran (Lab Scan, AR) were purified and distilled using standard procedures before use [15]. All other solvents and reagents were of analytical grade and were used as received.

2.2. Physical measurements and instrumentation

^{1}H-NMR spectra were recorded on a 300 MHz Bruker DPX300 FT-NMR spectrometer. Chemical shifts (δ ppm) were reported relative to tetramethylsilane (Me_4Si). Positive ion FAB mass spectra were

* Corresponding author. Tel.: +852-2859-2153; Fax: +852-2857-1586.
E-mail address: wwyam@hku.hk (V.W.-W. Yam).

0022-328X/03/$ - see front matter © 2003 Elsevier B.V. All rights reserved.
doi:10.1016/S0022-328X(03)00606-5

collected on a Finnigan MAT95 mass spectrometer. Positive ion and negative ion ESI mass spectra were collected on a Finnigan LCQ mass spectrometer. IR spectra were obtained as KBr pellets on a Bio-Rad FTS-7 Fourier-transform infrared spectrophotometer (4000–400 cm^{-1}). UV–Vis spectra were obtained on a Hewlett Packard 8452A diode array spectrophotometer. Steady-state excitation and emission spectra were obtained on a Spex Fluorolog 111 spectrofluorometer equipped with a Hamamatsu R-928 photomultiplier tube. Low-temperature (77 K) spectra were recorded by using an optical Dewar sample holder. Elemental analyses of the new complexes were performed on a Carlo Erba 1106 elemental analyzer at the Institute of Chemistry, Chinese Academy of Sciences.

Emission lifetime measurements were performed using a conventional laser system. The excitation source was the 355 nm output (third harmonic) of a Spectra-Physics Quanta-Ray Q-switched GCR-150 pulsed Nd-YAG laser (10 Hz). Luminescence decay signals were recorded on a Tektronix model TDS-620A (500 MHz, 2 GS/s) digital oscilloscope, and analyzed using a program for exponential fits. All solutions for photophysical studies were prepared under vacuum in a 10 cm^3 round-bottom flask equipped with a side-arm 1 cm fluorescence cuvette and sealed from the atmosphere by a Bibby Rotaflo HP6 Teflon stopper. Solutions were rigorously degassed with no fewer than four freeze-pump-thaw cycles.

2.3. Crystal structure determination

X-ray quality crystals of $[(dppm)_2Au_3\{C{\equiv}CC(=CH_2)Me\}_2][Au\{C{\equiv}CC(=CH_2)Me\}_2]$ (**14**) were obtained by recrystallization from dichloromethane-*n*-hexane. All the experimental details are given in Table 1. Crystal data for complex **14**: empirical formula, $[C_{70}H_{64}P_4Au_4]$; formula weight = 1817.04; monoclinic; space group, $P2_1/n$ (No. 14); $a = 14.299(2)$ Å; $b = 22.501(3)$ Å; $c = 19.906(3)$ Å; $\beta = 92.23(2)^\circ$; $V = 6399(1)$ $Å^3$; $Z = 4$; $D_{calc} = 1.886$ g cm^{-3}; μ(Mo–Kα) = 93.13 cm^{-1}; $F(0\,0\,0) = 3440$; $T = 301$ K. A colorless crystal of dimensions $0.40 \times 0.15 \times 0.10$ mm^3 inside a glass capillary was used for data collection at 28 °C on a MAR diffractometer with a 300 mm image plate detector using graphite monochromatized Mo–Kα radiation ($\lambda = 0.71069$ Å). 7169 reflections with $I > 3\sigma(I)$ were considered observed and used in the structural analysis. These reflections were in the range, h: 0–15; k: 0–27; l: −24–23 with $2\theta_{max} = 51^\circ$. The space group was determined based on a statistical analysis of intensity distribution and the successful refinement of structure solved by Patterson methods and expanded by Fourier methods (PATTY [16]) and refinement by full-matrix least-squares using the software package TEXSAN [17] on a Silicon Graphics Indy computer. The non-hydrogen atoms were refined anisotropically. Hydrogen atoms were included but not refined. Convergence for 703 variable parameters by least-squares refinement on F with $w = 4F_o^2/\sigma^2(F_o^2)$, where $\sigma^2(F_o^2) = [\sigma^2(I) + (0.040F_o^2)^2]$, for 7169 reflections with $I > 3\sigma(I)$ was reached at $R = 0.066$ and $wR = 0.084$ with a goodness-of-fit 1.85. The maximum and minimum peaks on the final difference Fourier map corresponded to −3.95 and 2.19 e $Å^{-3}$, respectively.

2.4. Syntheses

All reactions were carried out under anhydrous and anaerobic conditions under an inert atmosphere of nitrogen using standard Schlenk technique.

2.4.1. Synthesis of mononuclear gold(I) phosphine alkynyl complexes

2.4.1.1. [(Ph₃P)Au(C≡CC≡CC₃H₇)] (1). An ethanolic solution (5 ml) of 1,3-heptadiyne (20 mg, 0.21 mmol) and sodium ethoxide (0.30 mmol, prepared in situ from Na in EtOH) was added to a solution of [(Ph_3P)AuCl] (100 mg, 0.2 mmol) in EtOH–THF (10 ml; 1:1, v/v) and stirred at room temperature. The colourless solution

Table 1
Crystal and structure determination data for complex **14**

Empirical formula	$[C_{70}H_{64}P_4Au_4]$
Formula weight	1817.04
Crystal size (mm^3)	$0.40 \times 0.15 \times 0.10$
Crystal system	Monoclinic
Space group	$P2_1/n$
a (Å)	14.299(2)
b (Å)	22.501(3)
c (Å)	19.906(3)
α (°)	90
β (°)	92.23(2)
γ (°)	90
V ($Å^3$)	6399(1)
Z	4
$F(0\,0\,0)$	3440
M (cm^{-1})	93.13
D_{calc} (g cm^{-1})	1.886
Temperature (K)	301
Wavelength (Å)	0.71069
Collection range	$2\theta_{max} = 51.1^\circ$; h: 0–15, k: 0–27, l: −24–23
Reflections collected	11 163
No. of observations	7169
No. of variables	703
Refinement method	Full-matrix least-squares on F^2
Goodness-of-fit on F^2	1.85
Final R indices $[I > 3\sigma(I)]$[a]	$R_1 = 0.066$, $wR_2 = 0.084$
Largest difference peak and hole (e $Å^{-3}$)	2.19 and −3.95

[a] $w = 4F_o^2/\sigma^2(F_o^2)$, where $\sigma^2(F_o^2) = [\sigma^2(I) + (0.040F_o^2)^2]$ with $I > 3\sigma(I)$.

turned pale yellow after 30 min. After stirring for 4 h, the solvent was evaporated to dryness and the resulting solid was recrystallized from dichloromethane-*n*-hexane to give yellow crystals of **1** (45 mg, 41% yield). ^{1}H-NMR (300 MHz, $CDCl_3$, 298 K, relative to Me_4Si, δ ppm): 0.97 (t, 3H, $J = 7.3$ Hz, $-CH_3$), 1.36–1.46 (m, 2H, $-CH_2CH_2CH_3$), 2.30 (t, 2H, $J = 6.8$ Hz, $-C{\equiv}CCH_2-$), 7.45–7.61 (m, 15H, PPh_3). Positive ion FABMS; *m/z*: 525 $[M]^+$. IR (KBr disc, ν (cm^{-1})): 2209 (w, C≡C), 2141 (w, C≡C). Elemental analysis: Anal. Found: C, 52.18; H, 3.94. Calc. for $C_{25}H_{22}AuP \cdot 1/3CH_2Cl_2$: C, 52.59; H, 3.95%.

*2.4.1.2. [(Ph$_3$P)Au(C≡CC≡CC$_6$H$_{13}$)] (**2**).* The procedure was similar to that for **1** except 1,3-decadiyne (28 mg, 0.21 mmol) was used in place of 1,3-heptadiyne to give yellow crystals of **2** (41 mg, 35% yield). ^{1}H-NMR (300 MHz, $CDCl_3$, 298 K, relative to Me_4Si, δ ppm): 1.87 (t, 3H, $J = 7.1$ Hz, $-CH_3$), 1.27–1.57 (m, 8H, $-CH_2CH_2CH_2CH_2CH_3$), 2.25 (t, 2H, $J = 6.7$ Hz, $-C{\equiv}CCH_2-$), 7.46–7.57 (m, 15H, PPh_3). Positive ion FABMS; *m/z*: 593 $[M]^+$. IR (KBr disc, ν (cm^{-1})): 2201 (w, C≡C), 2140 (w, C≡C). Elemental analysis: Anal. Found: C, 56.85; H, 4.86. Calc. for $C_{28}H_{28}AuP$: C, 56.76; H, 4.76%.

*2.4.1.3. [(Ph$_3$P)Au(C≡CC≡CPh)] (**3**).* The procedure was similar to that for **1** except phenylbutadiyne (26 mg, 0.21 mmol) was used in place of 1,3-heptadiyne to give yellow crystals of **3** (39 mg, 33% yield). ^{1}H-NMR (300 MHz, $CDCl_3$, 298 K, relative to Me_4Si, δ ppm): 7.24–7.33 (m, 3H, –Ph), 7.45–7.57 (m, 17H, –Ph). Positive ion FABMS; *m/z*: 585 $[M]^+$. IR (KBr disc, ν (cm^{-1})): 2181 (w, C≡C), 2134 (w, C≡C). Elemental analysis: Anal. Found: C, 57.56; H, 3.55. Calc. for $C_{28}H_{20}AuP$: C, 57.55; H, 3.45%.

*2.4.1.4. [(Tol$_3$P)Au(C≡CC≡CPh)] (**4**).* The procedure was similar to that for **3** except [(Tol$_3$P)AuCl] (107 mg, 0.2 mmol) was used in place of [(Ph$_3$P)AuCl] to give yellow crystals of **4** (36 mg, 29% yield). ^{1}H-NMR (300 MHz, $CDCl_3$, 298 K, relative to Me_4Si, δ ppm): 2.38 (s, 9H, $-CH_3$), 7.23–7.53 (m, 17H, –Ph). Positive ion FABMS; *m/z*: 626 $[M]^+$. IR (KBr disc, ν (cm^{-1})): 2180 (w, C≡C), 2134 (w, C≡C). Elemental analysis: Anal. Found: C, 53.99; H, 3.99. Calc. for $C_{31}H_{26}AuP \cdot CH_2Cl_2$: C, 54.03; H, 3.97%.

2.4.2. Synthesis of dinuclear gold(I) phosphine alkynyl complexes

*2.4.2.1. [(dppe)Au$_2$(C≡CC≡CC$_6$H$_{13}$)$_2$] (**5**).* An ethanolic solution (5 ml) of 1,3-decadiyne (28 mg, 0.21 mmol) and sodium ethoxide (0.30 mmol, prepared in situ from Na in EtOH) was added to a solution of [(dppe)Au_2Cl_2] (87 mg, 0.1 mmol) in EtOH–THF (10 ml; 1:1, v/v) and stirred at room temperature. The colourless solution turned to pale yellow after 30 min. After stirring for 4 h, the solvent was evaporated to dryness and the resulting solid was recrystallized from dichloromethane-*n*-hexane to give orange crystals of **5** (61 mg, 58% yield). ^{1}H-NMR (300 MHz, $CDCl_3$, 298 K, relative to Me_4Si, δ ppm): 0.97 (t, 6H, $J = 7.2$ Hz, $-CH_3$), 1.25–1.65 (m, 16H, $-CH_2CH_2CH_2CH_2CH_3$), 2.31 (t, 4H, $J = 6.9$ Hz, $-C{\equiv}CCH_2-$), 2.62 (s, 4H, $-PCH_2CH_2P-$), 7.43–7.52 (m, 12H, $-PPh_2$), 7.63–7.77 (m, 8H, $-PPh_2$). Positive ion FABMS; *m/z*: 1058 $[M]^+$. IR (KBr disc, ν (cm^{-1})): 2203 (w, C≡C), 2140 (w, C≡C). Elemental analysis: Anal. Found: C, 54.65; H, 5.46. Calc. for $C_{46}H_{48}Au_2P_2 \cdot C_6H_{14}$: C, 54.65; H, 5.47%.

*2.4.2.2. [(dppe)Au$_2${C≡CC(=CH$_2$)Me}$_2$] (**6**).* The procedure was similar to that for **5** except 2-methylbut-1-en-3-yne (14 mg, 0.21 mmol) was used in place of 1,3-decadiyne to give air-stable pale orange crystals of **6** (61 mg, 66% yield). ^{1}H-NMR (300 MHz, $CDCl_3$, 298 K, relative to Me_4Si, δ ppm): 1.97(s, 6H, $-CH_3$), 2.59 (s, 4H, $-PCH_2CH_2P-$), 5.16 (d, 2H, $J = 1.9$ Hz, $=CH_2$), 5.32 (d, 2H, $J = 1.9$ Hz, $=CH_2$), 7.40–7.50 (m, 12H, $-PPh_2$), 7.53–7.64 (m, 8H, $-PPh_2$). Positive ion FABMS; *m/z*: 922 $[M]^+$. IR (KBr disc, ν (cm^{-1})): 2105 (w, C≡C). Elemental analysis: Anal. Found: C, 42.78; H, 3.59. Calc. for $C_{36}H_{34}Au_2P_2 \cdot 1.5CH_2Cl_2$: C, 42.89; H, 3.55%.

*2.4.2.3. [(dppf)Au$_2$(C≡CC$_4$H$_3$S)$_2$] (**7**).* The procedure was similar to that for **5** except [(dppf)Au_2Cl_2] (100 mg, 0.10 mmol) and 2-ethynylthiophene (23 mg, 0.21 mmol) were used in place of [(dppe)Au_2Cl_2] and 1,3-decadiyne, respectively, to give orange crystals of **7** (85 mg, 73% yield). ^{1}H-NMR (300 MHz, $CDCl_3$, 298 K, relative to Me_4Si, δ ppm): 4.29 (m, 4H, –Cp), 4.73 (m, 4H, –Cp), 6.92 (dd, 2H, $J = 1.2$ and 3.9 Hz, 3-thienyl protons), 7.12 (dd, 2H, $J = 3.9$ and 5.1 Hz, 4-thienyl protons), 7.18 (dd, 2H, $J = 1.2$ and 5.1 Hz, 5-thienyl protons), 7.41–7.55 (m, 20H, $-PPh_2$). Positive ion FABMS; *m/z*: 1055 $[M-(C{\equiv}CC_4H_3S)]^+$. IR (KBr disc, ν (cm^{-1})): 2097 (w, C≡C). Elemental analysis: Anal. Found: C, 45.29; H, 2.68. Calc. for $C_{46}H_{34}Au_2P_2S_2Fe \cdot CH_2Cl_2$: C, 45.25; H, 2.91%.

*2.4.2.4. [(dppf)Au$_2$(C≡CC$_4$H$_2$SC$_4$H$_3$S)$_2$] (**8**).* The procedure was similar to that for **5** except [(dppf)Au_2Cl_2] (100 mg, 0.10 mmol) and 5-ethynyl-2,2′-bithienyl (39 mg, 0.21 mmol) were used in place of [(dppe)Au_2Cl_2] and 1,3-decadiyne, respectively, to give orange crystals of **8** (77 mg, 68% yield). ^{1}H-NMR (300 MHz, $CDCl_3$, 298 K, relative to Me_4Si, δ ppm): 4.30 (m, 4H, –Cp), 4.73 (m, 4H, –Cp), 6.30 (d, 2H, $J = 4.1$ Hz, 4-bithienyl protons), 6.70 (d, 2H, $J = 4.1$ Hz, 3-bithienyl protons), 6.80 (dd, 2H, $J = 4.0$ and 5.3 Hz, 4′-bithienyl protons), 6.90 (dd, 2H, $J = 1.1$ and 4.0 Hz, 3′-bithienyl protons), 7.20 (dd, 2H, $J = 1.1$ and 5.3 Hz, 5′-bithienyl

protons), 7.42–7.56 (m, 20H, $-PPh_2$). Positive ion FABMS; *m/z*: 1137 $[M-(C{\equiv}CC_4H_2SC_4H_3S)]^+$. IR (KBr disc, *v* ($cm^{-1}$)): 2095 (w, C≡C). Elemental analysis: Anal. Found: C, 49.92; H, 3.56. Calc. for $C_{54}H_{38}Au_2P_2S_4Fe{\cdot}0.5C_6H_{14}$: C, 49.97; H, 3.31%.

2.4.3. Synthesis of trinuclear gold(I) phosphine alkynyl complexes

*2.4.3.1. [(dcpm)$_2$Au$_3$(C≡CC≡CC$_6$H$_{13}$)$_2$][Au(C≡CC≡CC$_6$H$_{13}$)$_2$] (**9**).* An ethanolic solution (5 ml) of 1,3-decadiyne (28 mg, 0.21 mmol) and sodium ethoxide (prepared in situ from Na in EtOH) was added to a solution of [(dcpm)Au_2Cl_2] (88 mg, 0.1 mmol) in EtOH–THF (10 ml; 1:1, v/v) and stirred at room temperature. The colourless solution turned to pale yellow after 30 min. After stirring for 4 h, the solvent was evaporated to dryness and the resulting solid was recrystallized from dichloromethane-*n*-hexane to give yellow crystals of **9** (70 mg, 33% yield). ^{1}H-NMR (300 MHz, $CDCl_3$, 298 K, relative to Me_4Si, δ ppm): 0.88 (t, 12H, $J = 7.2$ Hz, $-CH_3$), 1.25–1.58 (m, 72H, $-C_6H_{11}$; $-CH_2CH_2CH_2CH_2CH_3$), 1.80–2.04 (m, 48H, $-C_6H_{11}$), 2.30 (t, 8H, $J = 6.9$ Hz, $-C{\equiv}CCH_2-$). 3.65 (t, 4H, $J = 10.8$ Hz, $-PCH_2P-$). Positive ion FABMS; *m/z*: 1674 $[(dcpm)_2Au_3(C{\equiv}CC{\equiv}CC_6H_{13})_2]^+$. Positive ESIMS; *m/z*: 1674 $[(dcpm)_2Au_3(C{\equiv}CC{\equiv}CC_6H_{13})_2]^+$. Negative ESIMS; *m/z*: 463 $[Au(C{\equiv}CC{\equiv}CC_6H_{13})_2]^-$. IR (KBr disc, *v* ($cm^{-1}$)): 2141 (w, C≡C), 2060 (w, C≡C). Elemental analysis: Anal. Found: C, 49.42; H, 6.74. Calc. for $C_{90}H_{144}Au_4P_4{\cdot}CH_2Cl_2$: C, 49.17; H, 6.62%.

*2.4.3.2. [(dcpm)$_2$Au$_3${C≡CC(=CH$_2$)Me}$_2$][Au{C≡CC(=CH$_2$)Me}$_2$] (**10**).* The procedure was similar to that for **9** except 2-methylbut-1-en-3-yne (14 mg, 0.21 mmol) was used in place of 1,3-decadiyne to give pale yellow crystals of **10** (85 mg, 46% yield). ^{1}H-NMR (300 MHz, $CDCl_3$, 298 K, relative to Me_4Si, δ ppm): 1.15–1.80 (m, 56H, $-C_6H_{11}$), 1.85–2.10 (m, 32H, $-C_6H_{11}$, 12H, $-CH_3$), 2.31 (t, 4H, $J = 10.1$ Hz, $-PCH_2P-$), 5.03 (d, 4H, $J = 1.8$ Hz, $=CH_2$), 5.23 (d, 4H, $J = 1.8$ Hz, $=CH_2$). Positive ion FABMS; *m/z*: 1537 $[(dcpm)_2Au_3\{C{\equiv}CC(=CH_2)Me\}_2]^+$. Positive ESIMS; *m/z*: 1537 $[(dcpm)_2Au_3\{C{\equiv}CC-(=CH_2)Me\}_2]^+$. Negative ESIMS; *m/z*: 327 $[Au\{C{\equiv}CC(=CH_2)Me\}_2]^-$. IR (KBr disc, *v* ($cm^{-1}$)): 2102 (w, C≡C). Elemental analysis: Anal. Found: C, 44.31; H, 6.29. Calc. for $C_{70}H_{112}Au_4P_4{\cdot}2H_2O$: C, 44.20; H, 6.15%.

*2.4.3.3. [(dcpm)$_2$Au$_3$(C≡CC$_4$H$_3$S)$_2$][Au(C≡CC$_4$H$_3$S)$_2$] (**11**).* The procedure was similar to that for **9** except 2-ethynylthiophene (23 mg, 0.21 mmol) was used in place of 1,3-decadiyne to give pale yellow crystals of **11** (63 mg, 31% yield). ^{1}H-NMR (300 MHz, $CDCl_3$, 298 K, relative to Me_4Si, δ ppm): 1.25–1.54 (m, 40H, $-C_6H_{11}$) 1.73–2.17 (m, 48H, $-C_6H_{11}$), 2.25 (t, 4H, $J = 10.2$ Hz, $-PCH_2P-$), 6.84 (dd, 4H, $J = 1.2$ and 3.9 Hz, 3-thienyl protons), 7.09 (dd, 4H, $J = 3.9$ and 5.1 Hz, 4-thienyl protons), 7.10 (dd, 4H, $J = 1.2$ and 5.1 Hz, 5-thienyl protons). Positive ion FABMS; *m/z*: 1622 $[(dcpm)_2Au_3(C{\equiv}CC_4H_3S)_2]^+$. Positive ESIMS; *m/z*: 1621 $[(dcpm)_2Au_3(C{\equiv}CC_4H_3S)_2]^+$. Negative ESIMS; *m/z*: 412 $[Au(C{\equiv}CC_4H_3S)_2]^-$. IR (KBr disc, *v* ($cm^{-1}$)): 2105 (w, C≡C). Elemental analysis: Anal. Found: C, 43.75; H, 5.15. Calc. for $C_{74}H_{104}Au_4P_4S_4$: C, 43.70; H, 5.16%.

*2.4.3.4. [(dcpm)$_2$Au$_3$(C≡CC$_4$H$_2$SC$_4$H$_3$S)$_2$][Au(C≡CC$_4$H$_2$SC$_4$H$_3$S)$_2$] (**12**).* The procedure was similar to that for **9** except 5-ethynyl-2,2′-bithienyl (39 mg, 0.21 mmol) was used in place of 1,3-decadiyne to give yellow crystals of **12** (77 mg, 32% yield). ^{1}H-NMR (300 MHz, $CDCl_3$, 298 K, relative to Me_4Si, δ ppm): 1.25–1.58 (m, 40H, $-C_6H_{11}$), 1.80–2.04 (m, 48H, $-C_6H_{11}$), 2.22 (t, 4H, $J = 10.9$ Hz, $-PCH_2P-$), 6.48 (d, 4H, $J = 4.2$ Hz, 4-bithienyl protons), 6.87 (d, 4H, $J = 4.2$ Hz, 3-bithienyl protons), 7.15 (dd, 4H, $J = 3.9$ and 5.3 Hz, 4′-bithienyl protons), 7.39 (dd, 4H, $J = 1.2$ and 3.9 Hz, 3′-bithienyl protons), 7.67 (dd, 4H, $J = 1.2$ and 5.3 Hz, 5′-bithienyl protons). Positive ion FABMS; *m/z*: 1786 $[(dcpm)_2Au_3(C{\equiv}CC_4H_2SC_4H_3S)_2]^+$. Positive ESIMS; *m/z*: 1786 $[(dcpm)_2Au_3(C{\equiv}CC_4H_2SC_4H_3S)_2]^+$. Negative ESIMS; *m/z*: 575 $[Au(C{\equiv}CC_4H_2SC_4H_3S)_2]^-$. IR (KBr disc, *v* ($cm^{-1}$)): 2090 (w, C≡C). Elemental analysis: Anal. Found: C, 44.62; H, 4.73. Calc. for $C_{90}H_{112}Au_4P_4S_8{\cdot}CH_2Cl_2$: C, 44.66; H, 4.70%.

*2.4.3.5. [(dppm)$_2$Au$_3$(C≡CC≡CC$_6$H$_{13}$)$_2$][Au(C≡CC≡CC$_6$H$_{13}$)$_2$] (**13**).* The procedure was similar to that for **9** except [(dppm)Au_2Cl_2] (85 mg, 0.10 mmol) was used in place of [(dcpm)Au_2Cl_2] to give yellow crystals of **13** (70 mg, 34% yield) after recrystallized from chloroform-*n*-hexane. ^{1}H-NMR (300 MHz, $CDCl_3$, 298 K, relative to Me_4Si, δ ppm): 0.90 (t, 12H, $J = 7.1$ Hz, $-CH_3$), 1.28–1.65 (m, 32H, $-CH_2CH_2CH_2CH_2CH_3$), 2.30 (t, 8H, $J = 6.9$ Hz, $-C{\equiv}CCH_2-$), 3.65 (t, 4H, $J = 10.8$ Hz, $-PCH_2P-$), 7.38–7.58 (m, 24H, $-PPh_2$), 7.60–7.70 (m, 16H, $-PPh_2$). Positive ion FABMS; *m/z*: 1625 $[(dppm)_2Au_3(C{\equiv}CC{\equiv}CC_6H_{13})_2]^+$. Positive ESIMS; *m/z*: 1625 $[(dppm)_2Au_3(C{\equiv}CC{\equiv}CC_6H_{13})_2]^+$. Negative ESIMS; *m/z*: 463 $[Au(C{\equiv}CC{\equiv}CC_6H_{13})_2]^-$. IR (KBr disc, *v* ($cm^{-1}$)): 2139 (w, C≡C), 2054 (w, C≡C). Elemental analysis: Anal. Found: C, 45.71; H, 3.71. Calc. for $C_{90}H_{96}Au_4P_4{\cdot}3CHCl_3$: C, 45.70; H, 4.09%.

*2.4.3.6. [(dppm)$_2$Au$_3${C≡CC(=CH$_2$)Me}$_2$][Au{C≡CC(=CH$_2$)Me}$_2$] (**14**).* The procedure was similar to that for **9** except [(dppm)Au_2Cl_2] (85 mg, 0.10 mmol) and 2-methylbut-1-en-3-yne (14 mg, 0.21 mmol) were used in place of [(dcpm)Au_2Cl_2] and 1,3-decadiyne, respectively, to give air-stable pale yellow crystals of **14** (52 mg, 29% yield). ^{1}H-NMR (300 MHz, $CDCl_3$, 298

K, relative to Me_4Si, δ ppm): 1.95 (s, 12H, $-CH_3$), 3.56 (t, 4H, $J = 11.3$ Hz, $-PCH_2P-$), 5.08 (d, 4H, $J = 1.8$ Hz, $=CH_2$), 5.30 (d, 4H, $J = 1.8$ Hz, $=CH_2$), 7.30–7.50 (m, 24H, $-PPh_2$), 7.60–7.70 (m, 16H, $-PPh_2$). Positive FABMS; *m/z*: 1490 $[(dppm)_2Au_3\{C{\equiv}CC(=CH_2)Me\}_2]^+$. Positive ESIMS; *m/z*: 1489 $[(dppm)_2Au_3\{C{\equiv}CC(=CH_2)Me\}_2]^+$. Negative ESIMS; *m/z*: 327 $[Au\{C{\equiv}CC(=CH_2)Me\}_2]^-$. IR (KBr disc, ν (cm^{-1})): 2100 (w, C≡C). Elemental analysis: Anal. Found: C, 45.49; H, 3.33. Calc. for $C_{70}H_{64}Au_4P_4 \cdot 0.5CH_2Cl_2$: C, 45.54; H, 3.52%.

*2.4.3.7. [(dppm)$_2$Au$_3$(C≡CC$_4$H$_3$S)$_2$][Au(C≡CC$_4$H$_3$S)$_2$] (**15**).* The procedure was similar to that for **9** except $[(dppm)Au_2Cl_2]$ (85 mg, 0.10 mmol) and 2-ethynylthiophene (23 mg, 0.21 mmol) were used in place of $[(dcpm)Au_2Cl_2]$ and 1,3-decadiyne, respectively, to give pale yellow crystals of **15** (73 mg, 37% yield). ^{1}H-NMR (300 MHz, $CDCl_3$, 298 K, relative to Me_4Si, δ ppm): 3.62 (t, 4H, $J = 11.3$ Hz, $-PCH_2P-$), 6.90 (dd, 4H, $J = 1.2$ and 4.1 Hz, 3-thienyl protons), 7.06 (dd, 4H, $J = 3.9$ and 5.1 Hz, 4-thienyl protons), 7.19 (dd, 4H, $J =$ 1.2 and 5.1 Hz, 5-thienyl protons), 7.42–7.58 (m, 24H, $-PPh_2$), 7.68–7.73 (m, 16H, $-PPh_2$). Positive ion FABMS; *m/z*: 1467 $[M-(C{\equiv}CC_4H_3S)]^+$. Positive ESIMS; *m/z*: 1574 $[(dppm)_2Au_3(C{\equiv}CC_4H_3S)_2]^+$. Negative ESIMS; *m/z*: 412 $[Au(C{\equiv}CC_4H_3S)_2]^-$. IR (KBr disc, ν (cm^{-1})): 2093 (w, C≡C). Elemental analysis: Anal. Found: C, 44.53; H, 2.70. Calc. for $C_{74}H_{56}Au_4P_4S_4$: C, 44.77; H, 2.84%.

*2.4.3.8. [(dppm)$_2$Au$_3$(C≡CC$_4$H$_2$SC$_4$H$_3$S)$_2$][Au(C≡CC$_4$H$_2$SC$_4$H$_3$S)$_2$] (**16**).* The procedure was similar to that for **9** except $[(dppm)Au_2Cl_2]$ (85 mg, 0.10 mmol) and 5-ethynyl-2,2′-bithienyl (39 mg, 0.21 mmol) were used in place of $[(dcpm)Au_2Cl_2]$ and 1,3-decadiyne, respectively, to give yellow crystals of **16** (79 mg, 34% yield). ^{1}H-NMR (300 MHz, $CDCl_3$, 298 K, relative to Me_4Si, δ ppm): 3.60 (t, 4H, $J = 11.2$ Hz, $-PCH_2P-$), 6.73 (d, 4H, $J = 4.2$ Hz, 4-bithienyl protons), 6.92 (d, 4H, $J = 4.2$ Hz, 3-bithienyl protons), 7.05 (dd, 4H, $J =$ 3.9 and 5.3 Hz, 4′-bithienyl protons), 7.04 (dd, 4H, $J =$ 1.2 and 3.9 Hz, 3′-bithienyl protons), 7.11 (dd, 4H, $J =$ 1.2 and 5.3 Hz, 5′-bithienyl protons), 7.42–7.58 (m, 24H, $-PPh_2$), 7.68–7.73 (m, 16H, $-PPh_2$). Positive ion FABMS; *m/z*: 1743 $[(dppm)_2Au_3(C{\equiv}CC_4H_2SC_4H_3S)_2]^+$. Positive ESIMS; *m/z*: 1744 $[(dppm)_2Au_3(C{\equiv}CC_4H_2SC_4H_3S)_2]^+$. Negative ESIMS; *m/z*: 575 $[Au(C{\equiv}CC_4H_2SC_4H_3S)_2]^-$. IR (KBr disc, ν (cm^{-1})): 2093 (w, C≡C). Elemental analysis: Anal. Found: C, 45.60; H, 2.54. Calc. for $C_{90}H_{64}Au_4P_4S_8 \cdot CH_2Cl_2$: C, 45.57; H, 2.77%.

*2.4.3.9. [(dtpm)$_2$Au$_3${C≡CC(=CH$_2$)Me}$_2$][Au{C≡CC(=CH$_2$)Me}$_2$] (**17**).* The procedure was similar to that for **9** except $[(dtpm)Au_2Cl_2]$ (91 mg, 0.10 mmol) and 2-methylbut-1-en-3-yne (14 mg, 0.21 mmol) were used in place of $[(dcpm)Au_2Cl_2]$ and 1,3-decadiyne, respectively, to give air-stable pale yellow crystals of **17** (53 mg, 27% yield). ^{1}H-NMR (300 MHz, $CDCl_3$, 298 K, relative to Me_4Si, δ ppm): 1.95 (s, 12H, $-CH_3$), 2.35 (s, 24H, $-C_6H_4CH_3$), 3.43 (t, 4H, $J = 10.3$ Hz, $-PCH_2P-$), 5.09 (d, 4H, $J = 1.9$ Hz, $=CH_2$), 5.26 (d, 4H, $J = 1.9$ Hz, $=CH_2$), 7.17 (d, 16H, $J = 7.7$ Hz, $-C_6H_4-$), 7.53 (d, 16H, $J = 7.7$ Hz, $-C_6H_4-$). Positive ion FABMS; *m/z*: 1601 $[(dtpm)_2Au_3\{C{\equiv}CC(=CH_2)Me\}_2]^+$. Positive ESIMS; *m/z*: 1601 $[(dtpm)_2Au_3\{C{\equiv}CC(=CH_2)Me\}_2]^+$. Negative ESIMS; *m/z*: 327 $[Au\{C{\equiv}CC(=CH_2)Me\}_2]^-$. IR (KBr disc, ν (cm^{-1})): 2087 (w, C≡C). Elemental analysis: Anal. Found: C, 47.20; H, 4.13. Calc. for $C_{78}H_{80}Au_4P_4 \cdot CH_2Cl_2$: C, 47.11; H, 4.10%.

*2.4.3.10. [(dtpm)$_2$Au$_3$(C≡CC$_4$H$_3$S)$_2$][Au(C≡CC$_4$H$_3$S)$_2$] (**18**).* The procedure was similar to that for **9** except $[(dtpm)Au_2Cl_2]$ (91 mg, 0.10 mmol) and 2-ethynylthiophene (23 mg, 0.21 mmol) were used in place of $[(dcpm)Au_2Cl_2]$ and 1,3-decadiyne, respectively, to give pale yellow crystals of **18** (72 mg, 34% yield). ^{1}H-NMR (300 MHz, $CDCl_3$, 298 K, relative to Me_4Si, δ ppm): 2.37 (s, 24H, $-C_6H_4CH_3$), 3.47 (t, 4H, $J = 10.1$ Hz, $-PCH_2P-$), 6.84 (dd, 4H, $J = 1.2$ and 3.9 Hz, 3-thienyl protons), 7.03 (dd, 4H, $J = 3.9$ and 5.1 Hz, 4-thienyl protons), 7.19 (dd, 4H, $J = 1.2$ and 5.1 Hz, 5-thienyl protons), 7.20 (d, 16H, $J = 7.5$ Hz, $-C_6H_4-$), 7.50–7.62 (m, 16H, $-C_6H_4-$). Positive ion FABMS; *m/z*: 1685 $[(dtpm)_2Au_3(C{\equiv}CC_4H_3S)_2]^+$. Positive ESIMS; *m/z*: 1685 $[(dtpm)_2Au_3(C{\equiv}CC_4H_3S)_2]^+$. Negative ESIMS; *m/z*: 412 $[Au(C{\equiv}CC_4H_3S)_2]^-$. IR (KBr disc, ν (cm^{-1})): 2091 (w, C≡C). Elemental analysis: Anal. Found: C, 45.91; H, 3.36. Calc. for $C_{82}H_{72}Au_4P_4S_4 \cdot CH_2Cl_2$: C, 45.68; H, 3.42%.

*2.4.3.11. [(dmpm)$_2$Au$_3${C≡CC(=CH$_2$)Me}$_2$][Au{C≡CC(=CH$_2$)Me}$_2$] (**19**).* The procedure was similar to that for **9** except $[(dmpm)Au_2Cl_2]$ (60 mg, 0.10 mmol) and 2-methylbut-1-en-3-yne (14 mg, 0.21 mmol) were used in place of $[(dcpm)Au_2Cl_2]$ and 1,3-decadiyne, respectively, to give off-white crystals of **19** (47 mg, 39% yield). The complex would slowly decompose on standing in air at room temperature. ^{1}H-NMR (300 MHz, $CDCl_3$, 298 K, relative to Me_4Si, δ ppm): 1.74 (s, 6H, $-PCH_3$), 1.77 (s, 6H, $-PCH_3$), 1.87 (s, 6H, $-CH_3$), 1.89 (s, 6H, $-CH_3$), 2.07–2.15 (m, 12H, $-PCH_3$), 2.91 (t, 4H, $J = 10.9$ Hz, $-PCH_2P-$), 4.97 (d, 2H, $J = 2.0$ Hz, $=CH_2$), 5.07 (d, 2H, $J = 2.0$ Hz, $=CH_2$), 5.11 (d, 2H, $J =$ 2.0 Hz, $=CH_2$), 5.16 (d, 2H, $J = 2.0$ Hz, $=CH_2$). Positive ion FABMS; *m/z*: 993 $[(dmpm)_2Au_3\{C{\equiv}CC(=CH_2)Me\}_2]^+$. Positive ESIMS; *m/z*: 993 $[(dmpm)_2Au_3\{C{\equiv}CC(=CH_2)Me\}_2]^+$. Negative ESIMS; *m/z*: 327 $[Au\{C{\equiv}CC(=CH_2)Me\}_2]^-$. IR (KBr disc, ν (cm^{-1})): 2101 (w, C≡C). Elemental analysis: Anal.

Found: C, 20.35; H, 3.52. Calc. for $C_{20}H_{38}Au_4P_4$: C, 20.18; H, 3.22%.

*2.4.3.12. [(dmpm)$_2$Au$_3$(C≡CC$_4$H$_3$S)$_2$][Au(C≡CC$_4$H$_3$S)$_2$] (**20**).* The procedure was similar to that for **9** except [(dmpm)Au_2Cl_2] (60 mg, 0.10 mmol) and 2-ethynylthiophene (23 mg, 0.21 mmol) were used in place of [(dcpm)Au_2Cl_2] and 1,3-decadiyne, respectively, to give off-white crystals of **20** (42 mg, 28% yield). The complex was found to slowly decompose on standing in air at room temperature. ^{1}H-NMR (300 MHz, $CDCl_3$, 298 K, relative to Me_4Si, δ ppm): 1.71 (s, 12H, –PCH_3), 2.15 (s, 12H, –PCH_3), 2.93 (t, 4H, $J = 10.9$ Hz, –PCH_2P–), 6.87 (dd, 4H, $J = 1.2$ and 3.9 Hz, 3-thienyl protons), 6.99 (dd, 4H, $J = 3.9$ and 5.1 Hz, 4-thienyl protons), 7.09 (dd, 4H, $J = 1.2$ and 5.1 Hz, 5-thienyl protons). Positive ion FABMS; *m/z*: 1077 [(dmpm)$_2$Au$_3$(C≡CC$_4$H$_3$S)$_2$]$^+$. Positive ESIMS; *m/z*: 1077 [(dmpm)$_2$Au$_3$(C≡CC$_4$H$_3$S)$_2$]$^+$. Negative ESIMS; *m/z*: 411 [Au(C≡CC$_4$H$_3$S)$_2$]$^-$. IR (KBr disc, ν (cm^{-1})): 2091 (w, C≡C). Elemental analysis: Anal. Found: C, 26.86; H, 2.50. Calc. for $C_{34}H_{40}Au_4P_4S_4 \cdot CH_2Cl_2$: C, 26.71; H, 2.69%.

3. Results and discussion

3.1. Syntheses and characterization

The schematic drawings of the structures of the mono-, di-, and trinuclear gold(I) phosphine alkynyl complexes are summarized in Scheme 1. All the gold(I) complexes were prepared from the reaction of their chloro precursor complexes with organic alkynes in the presence of freshly prepared sodium ethoxide in EtOH–THF (1:1, v/v). The use of a mixed EtOH–THF (1:1, v/v) solvent, which renders the starting materials soluble in the reaction mixture, serves to provide a homogeneous medium for the reaction to occur. All the newly synthesized compounds gave satisfactory elemental analyses and have been characterized by ^{1}H-NMR spectroscopy, FABMS, ESIMS and IR spectroscopy. The structure of complex **14** was determined by X-ray crystallography.

The IR spectra of all the alkynyl complexes show weak absorption bands at ca. 2060–2200 cm^{-1}, typical of ν(C≡C) stretch of the alkynyl unit. In general, the monoynyl complexes show one ν(C≡C) stretch at ca. 2090–2105 cm^{-1} while the diynyl complexes show two ν(C≡C) stretches at ca. 2060–2200 cm^{-1}, characteristic of the terminal monoynyl and diynyl systems. The ^{1}H-NMR spectra of all the complexes show resonance signals and coupling patterns that are consistent with their chemical formulations. The identities of the trinuclear gold(I) alkynyl complexes have further been confirmed by ESIMS studies, in which both the trinuclear [(P^P)$_2$Au$_3$(C≡CR)$_2$]$^+$ cation and the [Au(C≡CR)$_2$]$^-$ counter-anion could be observed in the respective positive ESIMS and negative ESIMS detection mode.

3.2. Structural characterization

The perspective drawing of complex **14** is depicted in Fig. 1 and their selected bond distances and bond angles are collected in Table 2. The complex cation consists of three gold(I) atoms arranged in a triangular array with short Au···Au contacts of 3.1152(9), 3.1538(9) and 3.1490(9) Å, indicative of the presence of weak Au···Au interactions. Two of the gold(I) atoms were coordinated to one alkynyl carbon and one phosphorus atom, while the other gold(I) atom was coordinated to two phosphorus atoms of two dppm ligands. The counter-anion is a two-coordinate bis(alkynyl)gold(I). Similar findings have been observed in a related trinuclear complex [18]. The coordination geometry of all the gold atoms are essentially linear, typical of sp hybridization of gold(I), with P–Au–C bond angles (172.5(5)°, 171.8(5)°) showing a slight deviation from the ideal 180°, probably as a result of the steric demand of the ligands and crystal packing forces. The C≡C bond

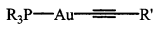

R	R'	
Ph	-C≡CC$_3$H$_7$	(1)
Ph	-C≡CC$_6$H$_{13}$	(2)
Ph	-C≡CPh	(3)
Tol	-C≡CPh	(4)

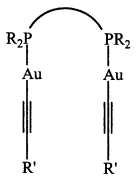

R$_2$P PR$_2$	R'	
dppe	-C≡CC$_6$H$_{13}$	(5)
dppe	-C(=CH$_2$)Me	(6)
dppf	-C$_4$H$_3$S	(7)
dppf	-C$_4$H$_2$SC$_4$H$_3$S	(8)

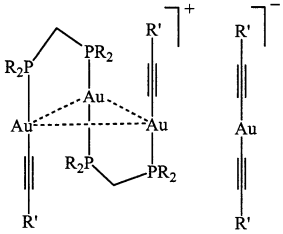

R	R'	
C$_6$H$_{11}$	-C≡CC$_6$H$_{13}$	(9)
C$_6$H$_{11}$	-C(=CH$_2$)Me	(10)
C$_6$H$_{11}$	-C$_4$H$_3$S	(11)
C$_6$H$_{11}$	-C$_4$H$_2$SC$_4$H$_3$S	(12)
Ph	-C≡CC$_6$H$_{13}$	(13)
Ph	-C(=CH$_2$)Me	(14)
Ph	-C$_4$H$_3$S	(15)
Ph	-C$_4$H$_2$SC$_4$H$_3$S	(16)
Tol	-C(=CH$_2$)Me	(17)
Tol	-C$_4$H$_3$S	(18)
Me	-C(=CH$_2$)Me	(19)
Me	-C$_4$H$_3$S	(20)

Scheme 1. Schematic drawings of complexes **1**–**20**.

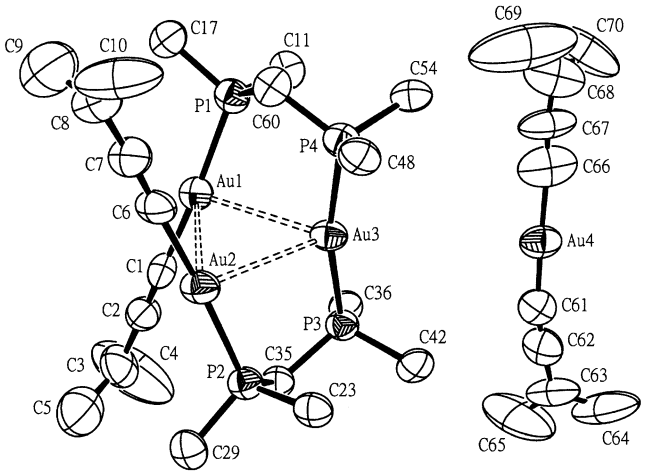

Fig. 1. Perspective view of complex **14** with atomic numbering. Only the *ipso*-carbons of the phenyl rings that are bonded to the phosphorus atoms are shown and hydrogen atoms have been omitted for clarity. Thermal ellipsoids are shown at 50% probability level.

lengths of 1.18(2), 1.22(2), 1.17(3) and 1.27(3) Å in **14** are typical of terminal alkynyl gold(I) systems [19,20].

3.3. Photophysical properties

3.3.1. Electronic absorption spectroscopy

3.3.1.1. Mononuclear gold(I) phosphine alkynyl complexes. The newly synthesized gold(I) alkynyl complexes in dichloromethane at room temperature are summarized in Table 3. The electronic absorption spectra of the mononuclear gold(I) complexes **1**–**4** in dichloromethane show high-energy absorption bands at ca. 250–270 nm, and low-energy absorptions at ca. 300–400 nm. The high-energy absorptions at ca. 250–270 nm, which are also present in the free phosphines, are assigned as phosphine-centered intraligand (IL) transitions. The intense absorptions at ca. 270–300 nm, which appear at similar energies as the absorptions of alkynes and show an energy dependence on the alkynyl ligands present, are assigned as IL $\pi \rightarrow \pi^*(C\equiv C)$ transition, while the less intense absorptions at ca. 300–400 nm, which also show an energy dependence on the nature of the alkynyl ligand, in which the energy follows the order: C≡CPh [21] > C≡C–C≡CC_3H_7 ≈ C≡C–C≡CC_6H_{13} > C≡C–C≡CPh that is in line with the π^* orbital energy of the alkynyl ligands, are tentatively assigned as metal-perturbed IL $\pi \rightarrow \pi^*(C\equiv C)$ transitions with some metal-to-alkynyl metal-to-ligand charge transfer (MLCT) character. This has further been supported by the observation of vibronic structures in the phenylbutadiynyl complexes **3** and **4**, with vibrational progressional spacings in the range 1730–2190 cm^{-1}, typical of $\nu(C\equiv C)$ in the excited state, and indicative of the involvement of the alkynyl ligand in the transition. Fig. 2 shows the electronic absorption spectrum of complex **3** in dichloromethane at 298 K. The relative insensitivity of the electronic absorption bands to the nature of the phosphine ligands, as reflected by the similar absorption patterns and energies of complexes **3** and **4**, is in line with the domination of IL $\pi \rightarrow \pi^*(C\equiv C)$ and metal-perturbed IL $\pi \rightarrow \pi^*(C\equiv C)$ transitions in the electronic absorption spectra.

Table 2
Selected bond distances (Å) and bond angles (°) for complex **14**

Bond distances	
Au(1)–Au(2)	3.1152(9)
Au(1)–Au(3)	3.1538(9)
Au(2)–Au(3)	3.1490(9)
Au(4)–C(61)	2.14(3)
Au(4)–C(66)	1.92(3)
C(61)–C(62)	1.17(3)
C(66)–C(67)	1.27(3)
Au(1)–C(1)	1.99(2)
Au(2)–C(6)	2.01(1)
C(1)–C(2)	1.18(2)
C(6)–C(7)	1.22(2)
Au(1)–P(1)	2.293(4)
Au(2)–P(2)	2.290(4)
Au(3)–P(3)	2.312(4)
Au(3)–P(4)	2.312(4)
Bond angles	
Au(1)–Au(2)–Au(3)	60.46(2)
Au(2)–Au(1)–Au(3)	60.30(2)
P(1)–Au(1)–C(1)	172.5(5)
P(2)–Au(2)–C(6)	171.8(5)
P(3)–Au(3)–P(4)	166.3(2)
Au(1)–C(1)–C(2)	175(2)
Au(2)–C(6)–C(7)	177(2)
Au(4)–C(61)–C(62)	175(3)
Au(4)–C(66)–C(67)	168(2)

3.3.1.2. Dinuclear gold(I) phosphine alkynyl complexes. The electronic absorption spectra of the dinuclear gold(I) complexes **5**–**8** in dichloromethane show intense high-energy absorptions at ca. 260–290 nm and less intense low-energy absorptions at ca. 300–440 nm.

The electronic absorption spectra of the dppe-containing dinuclear complexes **5** and **6** show similar absorption patterns as that of their mononuclear analogues. For example, the electronic absorption spectra of [(Ph_3P)Au{C≡CC(=CH_2)Me}] [6] and complex **6** are almost identical and are dominated by intense IL transitions, except that the dinuclear complex shows larger extinction coefficients for all the bands. Similarly, the high-energy absorption at ca. 260 nm is assigned as phosphine IL transitions. The intense absorptions at ca. 270–300 nm are likely to be typical of the alkynyl ligand and are assigned as IL $\pi \rightarrow \pi^*(C\equiv C)$ transitions. The observation of a higher absorption energy in complex **6** than complex **5** is in line with the poorer π conjugation in the enynyl group than in the hexadiynyl unit.

Table 3
Electronic absorption and emission data for complexes **1**–**20**

Complex	Absorption[a]	Emission	
	λ_{abs} (nm) (ε_{max}, $dm^3\ mol^{-1}\ cm^{-1}$)	Medium (T, K)	λ_{em} (nm) (τ_0, μs)
1	260 (18440), 278 (4440),	CH_2Cl_2 (298)	460 (< 0.1)
	318 sh (2250)	Solid (298)	464, 537, 595 (6.4)
		Solid (77)	480, 526, 594
2	264 (9000), 274 (2300),	CH_2Cl_2 (298)	454 (< 0.1)
	314 sh (540)	Solid (298)	460, 535, 594 (0.2)
		Solid (77)	474, 528, 600
3	252 (53350), 262 (48370),	CH_2Cl_2 (298)	460, 522, 590 (6.6)
	278 (36930), 296 (22340),	Solid (298)	468, 520, 590, 673 (4.3)
	314 (19140), 332 (9610),	Solid (77)	454, 528, 595
	358 (3600), 398 (560)		
4	252 (50220), 262 (43280),	CH_2Cl_2 (298)	466, 524, 591 (6.6)
	278 (27150), 296 (17360),	Solid (298)	481, 529, 596, 680 (2.0)
	314 (13180), 332 (5060),	Solid (77)	472, 528, 596
	358 (2060), 398 (230)		
5	260 (132270), 280 (33000),	CH_2Cl_2 (298)	420 (< 0.1)
	304 (11310), 316 sh (7320)	Solid (298)	552 (0.4)
		Solid (77)	476, 530, 555, 598
6	260 (53170), 270 (56420),	CH_2Cl_2 (298)	422 (0.7)
	298 sh (2880)	Solid (298)	625 (2.4)
		Solid (77)	478, 558
7	287 sh (37940), 298 (44530),	CH_2Cl_2 (298)	418 (< 0.1)
	312 sh (34510), 338 (3120),	Solid (298)	–[b]
	442 (240)	Solid (77)	–[b]
8	286 (47630), 298 (54260),	CH_2Cl_2 (298)	418 (< 0.1)
	314 (44110), 348 (8260),	Solid (298)	–[b]
	440 (270)	Solid (77)	–[b]
9	260 (105600), 270 (75540),	CH_2Cl_2 (298)	399 (0.7), 478, 533, 552, 600, 631 (3.4)
	304 (34650), 314 sh (9360)	Solid (298)	428 (0.3), 481, 507, 537, 560, 610, 630 (5.3)
		Solid (77)	440, 476, 531, 556, 600, 631
10	270 (38610), 282 (32790),	CH_2Cl_2 (298)	425 (0.3), 582 (1.2)
	314 sh (13070)	Solid (298)	425 (0.3), 610 (10.3)
		Solid (77)	420, 563, 621
11	256 (21950), 300 (23130),	CH_2Cl_2 (298)	418 (0.3), 499, 519 (3.0)
	312 sh (20330)	Solid (298)	423 (0.4), 535 (4.7)
		Solid (77)	418, 484, 496, 518, 538, 553, 581
12	280 (29250), 362 (50430),	CH_2Cl_2 (298)	429 (0.3)
	384 sh (36230)	Solid (298)	421 (0.2)
		Solid (77)	424
13	260 (89270), 270 (73130),	CH_2Cl_2 (298)	645 (3.9)
	304 (18090), 318 sh (5390)	Solid (298)	408 (0.5), 464, 538, 560, 606, 633 (3.0)
		Solid (77)	380,410, 480, 498,534, 555, 556, 602, 630
14	270 (36330), 294 (18270),	CH_2Cl_2 (298)	425 (0.7), 574 (1.6)
	310 sh (16210)	Solid (298)	425 (0.3), 600 (7.7)
		Solid (77)	425, 553, 580
15	252 (60240), 296 (32430),	CH_2Cl_2 (298)	410 (0.3), 499, 519 (7.5)
	312 sh (28330)	Solid (298)	421 (0.6), 525 (3.6)
		Solid (77)	418, 478, 492, 511, 528, 547, 570, 595
16	282 (27680), 356 (51370),	CH_2Cl_2 (298)	429 (0.2)
	386 sh (34130)	Solid (298)	420 (0.9)
		Solid (77)	424
17	276 (29050), 302 (14370),	CH_2Cl_2 (298)	427 (0.9), 589 (5.0)
	314 sh (2880)	Solid (298)	418 (0.8), 621 (3.9)
		Solid (77)	422, 630
18	258 (72370), 302 (55120),	CH_2Cl_2 (298)	440 (0.5), 500 (4.3)
	320 sh (32810)	Solid (298)	427 (0.4), 583 (1.2)
		Solid (77)	440, 476, 490, 510, 526, 544, 570, 592
19	270 (37310), 280 (28350),	CH_2Cl_2 (298)	425 (0.3), 618 (5.4)
	316 sh (11430)	Solid (298)	424 (0.4), 622 (2.7)
		Solid (77)	413, 622
20	250 (53570), 302 (61430),	CH_2Cl_2 (298)	416 (0.3), 503, 520 (5.8)

Table 3 (*Continued*)

Complex	Absorption[a]	Emission	
	λ_{abs} (nm) (ε_{max}, $dm^3\ mol^{-1}\ cm^{-1}$)	Medium (T, K)	λ_{em} (nm) (τ_0, μs)
	318 sh (34250)	Solid (298)	423 (0.2), 582 (2.2)
		Solid (77)	420, 500, 513, 535, 554, 576, 597

[a] In dichloromethane at 298 K.
[b] Non-emissive.

On the other hand, intense vibronic-structured bands at 262–298 nm were observed in the electronic absorption spectra of the dppf-containing complexes **7** and **8**. Fig. 3 depicts the electronic absorption spectrum of complex **7** recorded in dichloromethane at 298 K. The vibrational progressional spacings in the range 1280–1560 cm^{-1} are typical of ν(C---C) stretch in the excited state. The large extinction coefficients in the order of 10^5 $dm^3\ mol^{-1}\ cm^{-1}$ suggested that the transitions involve IL $\pi \rightarrow \pi^*$(C---C) transitions, probably associated with both the cyclopentadienyl and the thiophene moieties. In addition, the complexes display a low-energy absorption shoulder at ca. 300–350 nm, similar to that observed in other related dppf-containing complexes such as [(dppf)Au_2(C≡CPh)$_2$] and [(dppf)Au_2(C≡C^{t}Bu)$_2$] [20]. With reference to previous spectroscopic studies [20], this shoulder is assigned as a $\sigma \rightarrow \pi^*$(Ar) transition of the dppf ligands (σ refers to the bonding orbital of Au–P σ bond and π^*(Ar) denotes the antibonding molecular orbital of the phenyl ring in the PPh_2 units or Cp of dppf). Furthermore, the complexes show a weak absorption at ca. 440 nm with extinction coefficients of 210–270 $dm^3\ mol^{-1}\ cm^{-1}$. Similar findings have been observed in the absorption characteristics of other related ferrocene-containing complexes [20] including the [Au_2(dppf)Cl_2] precursor, which is typical of the ferrocene moiety.

The close resemblance of the electronic absorption patterns of the mono- and dinuclear complexes and the larger extinction coefficients observed in the dinuclear species suggest that the two Au units in the dinuclear species are non-interacting in nature and can be treated as two independent chromophores.

3.3.1.3. Trinuclear gold(I) phosphine alkynyl complexes. When comparing the trinuclear Au(I) complexes with the same alkynyl ligands, the electronic absorption spectra appeared to be very similar. Similar to the mononuclear Au(I) alkynyl complexes, it appears that in the trinuclear system a change in the phosphine ligand imposes insignificant changes on both the high-energy and low-energy absorption bands. On the contrary, the electronic absorption spectra of the trinuclear complexes with different alkynyl ligands show different absorption patterns. In general, an absorption energy trend in line with the π^* orbital energy of the C≡CR′ unit is observed, in which $R' = C(=CH_2)Me \approx C_4H_3S > C_4H_2SC_4H_3S$.

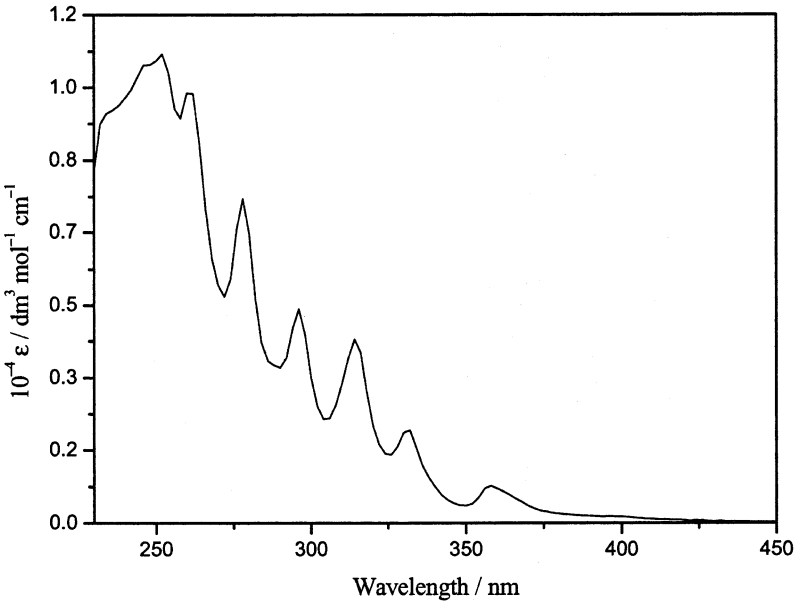

Fig. 2. Electronic absorption spectrum of **3** in dichloromethane at 298 K.

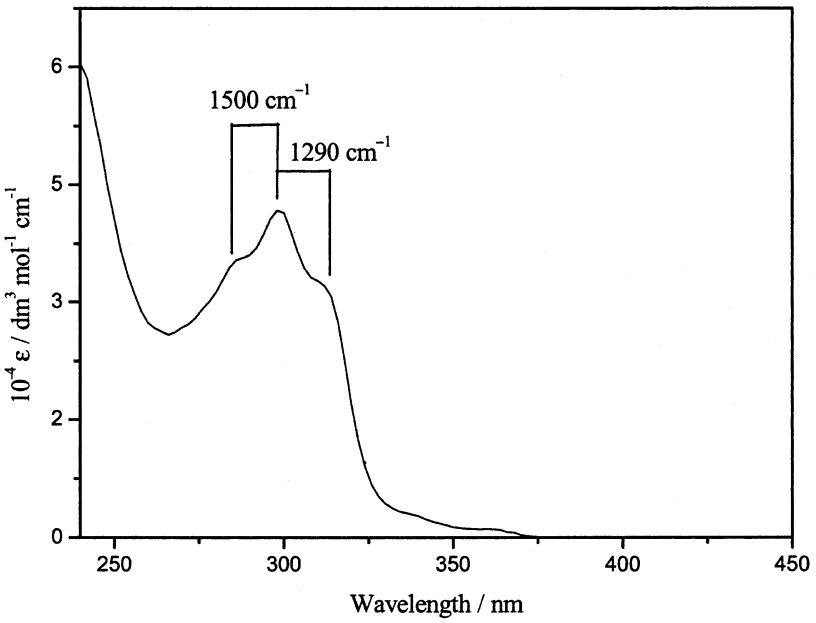

Fig. 3. Electronic absorption spectrum of **7** in dichloromethane at 298 K.

The electronic absorption spectra of the oligothienyl substituted alkynyl complexes **15** and **16** in dichloromethane at 298 K are shown in Fig. 4. The electronic absorptions at 294–302 nm for the thienyl complexes and 360–362 nm for the bithienyl complexes are assigned as thiophene-based $\pi \rightarrow \pi^*$ and $n \rightarrow \pi^*$ transitions of the respective $C{\equiv}CC_4H_3S$ and $C{\equiv}CC_4H_2SC_4H_3S$ units. The low-energy absorption shoulders at ca. 310 nm in the thienyl complexes and at ca. 380 nm in the bithienyl complexes are likely to involve metal-perturbed IL $\pi \rightarrow \pi^*(C{\equiv}C)$ transitions. The red shift in absorption energies of the bithienyl complexes relative to their thienyl counterparts is in line with an increase in the extent of π-conjugation in the bithienyl unit, which will cause a narrowing of the $\pi \rightarrow \pi^*$ energy gap.

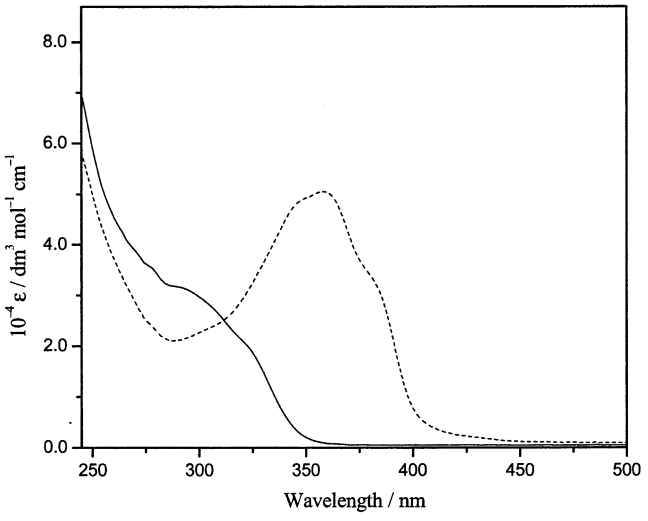

Fig. 4. Electronic absorption spectra of complexes 15 (—) and 16 (---) in dichloromethane at 298 K.

3.3.1.4. Effect of nuclearity. In order to study the effect of nuclearity of the metal complexes on their electronic absorption spectroscopy, a comparison of the electronic absorption spectra of the mononuclear, dinuclear and trinuclear Au(I) complexes is desirable. As an illustration, the mononuclear complex, $[(Ph_3P)Au\{C{\equiv}CC(=CH_2)Me\}]$ [6] or $[(Tol_3P)Au\{C{\equiv}CC(=CH_2)Me\}]$ [6], and their dinuclear analogue **6** and trinuclear analogue **14** were chosen. Although the phosphines employed in the mono-, di- and trinuclear complexes are not exactly identical, a comparison study is still possible, given the insignificant effect of the phosphines on the electronic absorption properties of the complexes as discussed earlier. The electronic absorption spectra of $[(Ph_3P)Au\{C{\equiv}CC(=CH_2)Me\}]$ [6], **6**, and **14** in dichloromethane at 298 K are depicted in Fig. 5. The electronic absorption spectra are all very similar and are dominated by intense absorptions at ca. 258–280 nm, typical of IL transitions of the phosphines and the alkynyl ligands. It is interesting to note that the extinction coefficients of these high-energy absorptions increase with an increase in the nuclearity of the complexes from $[(Ph_3P)Au\{C{\equiv}CC(=CH_2)Me\}]$ to **6** to **14**, in line with the increase in the number of the chromophoric units according to the additivity rule. A close scrutiny of the low-energy region at ca. 290–316 nm shows that there are differences. A red shift in the absorption shoulder/tail is observed on going from the mono- and dinuclear complexes to the trinuclear species. The observation of short Au···Au contacts in the trinuclear Au(I) complexes, as reflected by the X-ray study on

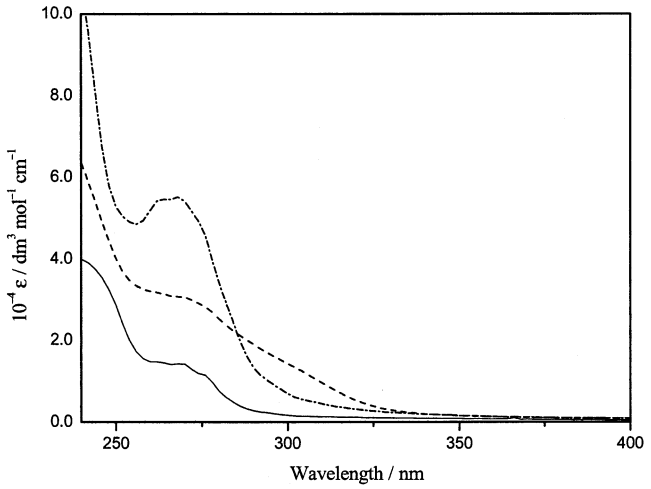

Fig. 5. Electronic absorption spectra of [(PPh_3)Au{C≡CC(=CH_2)Me}] (—), **6** (---) and **14** (-·-·-·) in dichloromethane at 298 K.

[$(dppm)_2Au_3${C≡CC(=CH_2)Me}$_2$][Au{C≡CC(=CH_2)Me}$_2$] (**14**) and that previously reported on a related [$(dppm)_2Au_3$(C≡CPh)$_2$][Au(C≡CPh)$_2$] [18], suggests that weak Au···Au interactions exist in these complexes. This would lead to d_z^2(Au)–d_z^2(Au) orbital overlap to give dσ and dσ* combinations, raising the energy of the metal-centered dσ* orbital which has a substantial character in the HOMO. Thus, a red shift in the transition with large metal-to-alkynyl MLCT character due to the presence of metal–metal interactions or a metal-metal-to-ligand charge transfer (MMLCT) transition is observed. On the other hand, the similarity in the shapes between the electronic absorption spectra of the mononuclear and the dinuclear complexes bridged by the dppe or dppf ligand is suggestive of the absence of short Au···Au contacts in the dinuclear complexes, as evidenced by the absence of Au···Au interactions in a related [(dppe)Au_2(C≡CPh)$_2$] [21a] and [(dppf)Au_2{C≡CC(=CH_2)Me}$_2$] [6]. Thus, the two Au(C≡CR′) units in the dinuclear complexes would behave as independent entities, giving rise to similar absorption energies as the mononuclear counterparts.

3.3.2. Steady-state emission spectroscopy

Excitation of the gold(I) phosphine alkynyl complexes both in the solid state and in fluid solutions showed long-lived luminescence. The photophysical data are summarized in Table 3.

3.3.2.1. Mononuclear gold(I) phosphine alkynyl complexes. The mononuclear gold(I) phosphine alkynyl complexes exhibit intense vibronic-structured emissions at room temperature at ca. 460–680 nm in the solid state upon photoexcitation with $\lambda > 350$ nm. Their luminescence lifetimes in the microsecond range suggested that the emissions are phosphorescence in nature. Vibronic structures with vibrational progressional spacings of ca. 2100 cm^{-1}, typical of the ν(C≡C) stretch in the ground state, were observed in the solid-state emission spectra of **1**–**4** both at room temperature and at 77 K. Fig. 6 displays the solid-state emission spectrum of complex **3** at 298 K. This is indicative of the involvement of the alkynyl unit in the emissive state.

The solid-state emission maxima for complexes **1** and **2** were found to be very similar while complexes **3** and **4** were found to occur at different energies with emission maxima at 468 and 481 nm, respectively. An emission energy trend of **4** < **3** < **2** ≅ **1** was observed. The similar emission energies of **1** and **2** are in agreement with the similar π-acceptor abilities of the heptadiynyl and decadiynyl units. The red shift in emission energies from **1** and **2** to **3** and **4** is in line with the low-lying π*(C≡C) orbital energy of C≡C–C≡CPh than C≡C–C≡CC_nH_{2n+1}, suggestive of an assignment of the emissive state as derived from states of a σ(Au–P) → π*(C≡C) character, or a metal-perturbed IL π → π*(C≡C) origin with MLCT character. The slight red shift in emission energy on going from PPh_3 in **3** to $PTol_3$ in **4** is consistent with an assignment of the emissive state as derived from a ^{3}(σ → π*) transition associated with the [Au(C≡CR)] groups, since $PTol_3$, being a better electron donor than PPh_3, would render the gold(I) center more electron rich, making the ^{3}[σ(Au–P) → π*(C≡C)] or metal-perturbed ^{3}IL [π → π*(C≡C)]/^{3}MLCT excited state low-lying in energy. Similar trends have been observed in the 77 K solid-state emission energies. A comparison of the emission energies of **1**–**4** with other related complexes shows that the emission energies of [(R_3P)Au(C≡CR′)] in 77 K solid state are in the order: R′ = C≡CPh ≈ C(=CH_2)Me [6] < Ph [21] and C≡CPh < C≡CC_3H_7 ≈ C≡CC_6H_{13} < C(=CH_2)Me [6], in line with the increasing π* orbital energy of the alkynyl group. This is also supportive of an assignment of the emissive states as derived from states of a ^{3}[σ(Au–P) → π*(C≡C)]

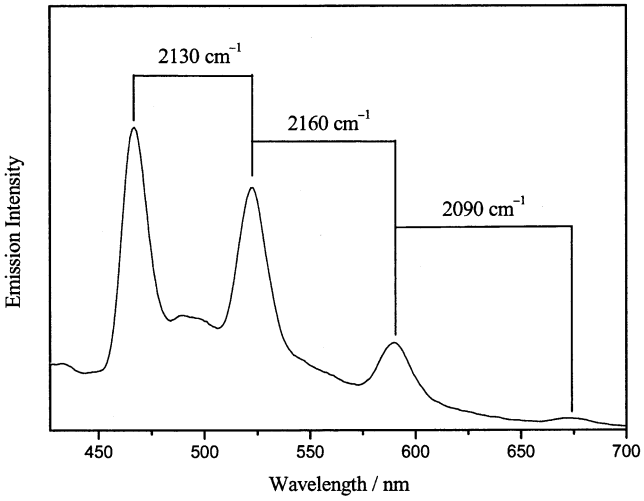

Fig. 6. Solid-state emission spectrum of complex **3** at 298 K.

character, or a metal-perturbed ^{3}IL [$\pi \rightarrow \pi^*$(C≡C)] mixed with a MLCT ^{3}MLCT character. In solution state, the complexes emit at ca. 454–590 nm, also dependent on the nature of the alkynyl ligand.

3.3.2.2. Dinuclear gold(I) phosphine alkynyl complexes. For the dinuclear dppe-containing gold(I) complexes **5** and **6**, complex **5** was found to emit at 552 nm in the solid state at 298 K, while complex **6** was found to emit at 625 nm. In degassed dichloromethane solutions, both **5** and **6** emit at ca. 420 nm. The anomalous observation that the diynyl complex **5** emits at higher energy than the enynyl complex **6** in the solid state at 298 K may be attributed to solid-state effects. Although no X-ray quality crystals could be obtained for the structure determination of complexes **5** and **6**, based on previous studies on a related complex [(dppe)Au_2(C≡CPh)$_2$] [21a], which consists of two weakly interacting molecules in an anti-configuration, with intermolecular Au–Au distance of 3.153(2) Å, one may assume that complex **6**, similar to the [(dppe)Au_2(C≡CPh)$_2$] analogue, may possess short intermolecular Au···Au contacts, and gives rise to low-energy solid-state emission, typical of the presence of Au···Au interaction. Although no short intramolecular Au···Au contact exists, it is likely that the presence of an intermolecular short Au···Au contact in **6** would also give rise to an Au···Au interaction in the solid state. On the other hand, it is likely that no short Au···Au contacts, both intra- and intermolecular, exist in the solid-state structure of the diynyl complex **5** since the long alkyl chains present may induce a steric hindrance with the adjacent molecules to prevent any close Au···Au contacts to occur. The low-energy emission of **6** is tentatively assigned as a metal-perturbed ^{3}IL [π(C≡C) $\rightarrow \pi^*$(C≡C)] emission modified by metal–metal interactions or an MMLCT ^{3}[d$\sigma^*(Au_2) \rightarrow \pi^*$(C≡C)] emission. Fig. 7 shows the emission spectra of complex **6** in the solid state and in dichloromethane solution. The absence of low-energy emission in CH_2Cl_2 solution is attributed to the absence of short Au···Au contacts in solution and IL phosphorescence becomes dominant.

For the dinuclear dppf-containing gold(I) complexes **7** and **8**, no emission was detected in the solid-state both at 298 and 77 K. A weak emission at ca. 418 nm was observed in degassed dichloromethane solutions. With reference to previous spectroscopic studies on [(dppf)Au_2(C≡CPh)$_2$] and [(dppf)Au_2(C≡C^{t}Bu)$_2$] [20], the emission is assigned to be originated from a σ(Au–P) $\rightarrow \pi^*$(Ar) excited state, of which σ refer to the P–Au bonding orbital and π^* refers to the antibonding orbital of the phenyl or cyclopentadienyl ring on the phosphine ligands. The lack of emission in the solid-state is probably a result of the introduction of the ferrocenyl unit, which would quench the emission via an intramolecular reductive electron transfer quenching process.

3.3.2.3. Trinuclear gold(I) phosphine alkynyl complexes. For the trinuclear Au(I) complexes, two emission bands were observed. The high-energy band is at ca. 400–480 nm, whereas the low-energy one appears at ca. 500–622 nm. In the two series **9**–**12** and **13**–**16** that have the same kind of diphosphine ligands dcpm or dppm, the emission energy follows the order: C≡CC_4H_3S > C≡CC(=CH_2)Me > C≡CC≡CC_6H_{13}, in line with the decreasing π^* orbital energy of the alkynyl ligands, and similar to the trend observed in the electronic absorption spectra. This is supportive of an assignment of the emissive states as derived from states of a σ(Au–P) $\rightarrow \pi^*$(C≡C) transition, or a metal-perturbed IL [$\pi \rightarrow \pi^*$(C≡C)] transition with MLCT ^{3}MLCT character. The only exception is complexes **12** and **16** with bithienyl ligand, in which no emission band was found at 530–600 nm. It is likely that the introduction of bithienyl groups into the Au(I) complexes quenches the emissive state, with the low-energy emission band becomes undetectable.

The high-energy band, which is more intense than the low-energy band, is logically assigned to be originated from the anion as emission bands of similar energies are observed in the [Au(C≡CR)$_2$]$^-$ [21a]. The low-energy emission bands, which are red shifted with respect to that of the corresponding mono- and dinuclear species, are likely to be associated with the presence of metal–metal interactions in the trinuclear complexes. The observation of short Au···Au contacts in the trinuclear Au(I) complexes, as reflected by X-ray study on complex **14** and that previously reported on a related [(dppm)$_2Au_3$(C≡CPh)$_2$][Au(C≡CPh)$_2$] [18], suggests that weak Au···Au interactions exist in these complexes. This would lead to a d_z^2(Au)–d_z^2(Au) orbital overlap to give dσ and dσ^* combinations, raising the energy of the metal-centered dσ^* orbital which has substantial character in the HOMO. Thus, the observation of the low-

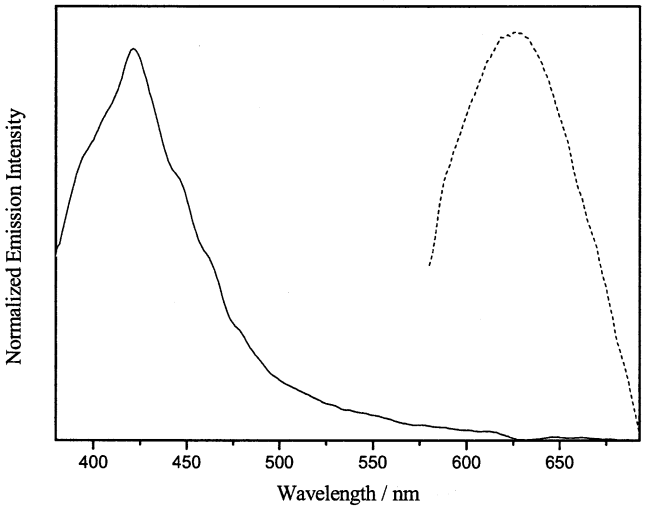

Fig. 7. Normalized emission spectra of complex **6** in the solid state (—) and in degassed dichloromethane solution (---) at 298 K.

energy emission in the trinuclear complex is in accordance with the presence of weak Au···Au interactions in these trinuclear complexes, which gave rise to low-energy emission that is of a metal-perturbed IL [$\pi \rightarrow \pi^*$(C≡C)] mixed with a metal-to-alkynyl MLCT character modified by metal–metal interactions, or an MMLCT nature.

3.3.2.4. Effect of phosphine substituents. When considering the influence of the phosphine ligands on the emission energy of the trinuclear Au(I) complexes, the high-energy emission does not seem to be much affected by the nature of the phosphine ligands. This is further supportive of an assignment that the origin of this emission is from the $[Au(C{\equiv}CR)_2]^-$ anion. On the other hand, the low-energy emission follows a subtle emission energy trend of dppm > dtpm ≈ dcpm > dmpm, in line with an emission origin of $^3[\sigma(Au-P) \rightarrow \pi^*(C{\equiv}C)]$ or metal-perturbed ^{3}IL [$\pi \rightarrow \pi^*$(C≡C)] excited states. Since dtpm, dcpm and dmpm are more electron-rich than dppm, they would render the gold(I) center more electron-rich, and hence give rise to a lower energy $^3[\sigma(Au-P) \rightarrow \pi^*(C{\equiv}C)]$ emission.

3.3.2.5. Effect of nuclearity. In order to study the effect of nuclearity of the metal complexes on their emission spectroscopy, a comparison of the emission spectra of the mononuclear Au(I) complexes, i.e. [$(Ph_3P)Au\{C{\equiv}CC(=CH_2)Me\}$] [$\lambda_{em}$(solid state) ≅ 454 nm] or [$(Tol_3P)Au\{C{\equiv}CC(=CH_2)Me\}$] [$\lambda_{em}$(solid state) ≅ 463 nm] [6], with that of the dinuclear complex **6** and the trinuclear complex **14** was made. Fig. 8 shows the solid-state emission spectra of **6** and **14** at 298 K.

For the solid-state emission spectra, the similarity in the shapes and emission energies (600–625 nm) of the band between complexes **6** and **14** is suggestive of their common emission origin. It is likely that the presence of short Au···Au contacts in both the trinuclear and dinuclear Au(I) complexes, as reflected by X-ray study and that previously reported on the related $[(dppm)_2Au_3(C{\equiv}CPh)_2][Au(C{\equiv}CPh)_2]$ [18] and $[(dppe)Au_2(C{\equiv}CPh)_2]$ [21a], whether intra- or intermolecular in nature, would give rise to weak Au···Au interactions in these complexes. This would lead to a d_z^2(Au)–d_z^2(Au) orbital overlap to give dσ and dσ* combinations, raising the energy of the metal-centered dσ* orbital which has substantial character in the HOMO. Thus, a red shift in the $^3[\sigma(Au-P) \rightarrow \pi^*(C{\equiv}C)]$ or the metal-perturbed ^{3}IL [$\pi \rightarrow \pi^*$(C≡C)] mixed with metal-to-alkynyl ^{3}MLCT modified by metal–metal interactions, or the MMLCT ^{3}MMLCT emission energy is observed relative to that of the mononuclear complexes. This is understandable since the absence of short Au···Au contacts in the mononuclear complexes would give rise to a higher energy emission that is mainly derived from a $\sigma(Au-P) \rightarrow \pi^*(C{\equiv}C)$ excitation.

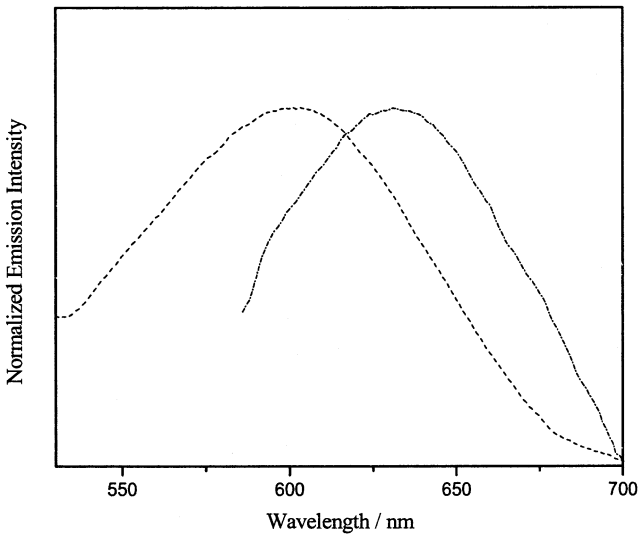

Fig. 8. Normalized solid-state emission spectra of **6** (-···-·), and **14** (---) at 298 K.

It is interesting to note that the low-energy emission band persists in the trinuclear complexes in the solution state, while the low-energy emission band disappears in the dinuclear complexes in solution. It is likely that the intramolecular Au···Au interaction remains intact in solution in the trinuclear complexes while in the dinuclear system, the intermolecular Au···Au interactions are destroyed in solution and their emission resembles that of their mononuclear counterpart.

4. Conclusion

A series of mono-, di- and trinuclear gold(I) phosphine alkynyl complexes has been synthesized and structurally characterized. In general, the high-energy absorptions are due to IL phosphine-centered and $\pi \rightarrow \pi^*$(C≡C) transitions, whereas the low-energy absorptions are assigned as $\sigma(Au-P) \rightarrow \pi^*(C{\equiv}C)$ or metal-perturbed IL $\pi \rightarrow \pi^*$(C≡C) mixed with metal-to-alkynyl MLCT transitions. Both the electronic absorption and emission energies are found to depend on the nature of the alkynyl ligands. The nuclearity of the metal complexes also has an influence on the electronic absorption as well as emission behavior. The emission energies are generally found to be lowest in the trinuclear complexes, attributed to the presence of weak Au···Au interactions.

5. Supplementary material

Crystallographic data for the structural analysis have been deposited with the Cambridge Crystallographic Data Centre, CCDC No. 213084 for complex **14**. Copies of this information may be obtained free of charge from

The Director, CCDC, 12 Union Road, Cambridge CB2 1EZ, UK (Fax: +44-1223-336033; e-mail: deposit@ccdc.cam.ac.uk or www: http://www.ccdc.cam.ac.uk).

Acknowledgements

V.W.-W.Y. acknowledges support from The University of Hong Kong Foundation for Educational Development and Research. The work described in this paper has been supported by the Research Grants Council of the Hong Kong Special Administrative Region, China (Project No. HKU7123/00P). K.-L.C. and S.-K.Y. acknowledge the receipt of a postgraduate studentship, administered by The University of Hong Kong.

References

[1] (a) S.R. Marder, J.E. Sohn, G.D. Stucky (Eds.), Materials for Nonlinear Optics: Chemical Perspectives, ACS Symp. Ser. 455, American Chemical Society, Washington DC, 1991;
(b) D.W. Bruce, D. O'Hare, Inorganic Materials, Wiley, Chichester, UK, 1992;
(c) R.M. Laine (Ed.), Inorganic and Organometallic Polymers with Special Properties, Kluwer Academic Publishers, Dordrecht, 1990;
(d) M.H. Lyons (Ed.), Materials for Non-linear and Electro-optics 1989, The Institute of Physics, Bristol, 1989;
(e) G. Marr, B.W. Bockett, in: S. Patai, F.R. Hartley (Eds.), The Chemistry of the Metal Carbon Bond, Wiley/Interscience, Chichester, UK, 1982;
(f) G. Khanarian (Ed.), Nonlinear Optical of Organic Molecules, SPIE, Bellingham, 1988.

[2] (a) J.L. Bredas, R.R. Chance (Eds.), Conjugated Polymer Materials: Opportunities in Electronic, Optoelectronic and Molecular Electronics, NATO ASI Series 182, Kluwer, Dordrecht, 1990;
(b) D.L. Mills, Nonlinear Optics, Springer-Verlag, Berlin, 1991;
(c) R.W. Munn, C.N. Ironside, Principles and Applications of Nonlinear Optical Materials, Blackie, Glasgow, 1993.

[3] (a) D.J. Williams, Angew. Chem. Int. Ed. Engl. 23 (1984) 690;
(b) N.J. Luong, Angew. Chem. Int. Ed. Engl. 34 (1995) 21.

[4] (a) M.I. Bruce, D.A. Harbourne, F. Waugh, F.G.A. Stone, J. Chem. Soc. A (1968) 356;
(b) N. Hagihara, K. Sonogashira, S. Takahashi, Adv. Polym. Sci. 41 (1981) 151.

[5] (a) T. Müller, S.W.K. Choi, D.M.P. Mingos, D. Murphy, D.J. Williams, V.W.-W. Yam, J. Organomet. Chem 484 (1994) 209;
(b) V.W.-W. Yam, S.W.K. Choi, J. Chem. Soc. Dalton Trans., (1996) 4227;
(c) C.M. Che, H.Y. Chao, V.M. Miskowski, Y. Li, K.-K. Cheung, J. Am. Chem. Soc. 123 (2001) 4985;
(d) W. Lu, H.F. Xiang, N. Zhu, C.M. Che, Organometallics 21 (2002) 2343.

[6] V.W.-W. Yam, K.-L. Cheung, C.C. Cheng , N. Zhu, K.-K. Cheung, J. Chem. Soc. Dalton Trans. (2003) 1830.

[7] (a) C.F. Shaw, in: H. Schmidbauer (Ed.), Gold: Progress in Chemistry, Biochemistry, and Technology, Wiley, New York, 1999, p. 259;
(b) D.M.P. Mingos, R. Vilar, D. Rais, J. Organomet. Chem. 641 (2002) 126;
(c) V.W.-W. Yam, K.-L. Cheung, L.H. Yuan, K.M.C. Wong, K.-K. Cheung, Chem. Commun. 16 (2000) 1513;
(d) W.J. Hunks, M.A. MacDonald, M.C. Jennings, R.J. Puddephatt, Organometallics 19 (2000) 5063;
(e) C.P. McArdle, S. Van, M.C. Jennings, R.J. Puddephatt, J. Am. Chem. Soc. 124 (2002) 3959;
(f) F. Mohr, D.J. Eisler, C.P. McArdle, K. Atieh, M.C. Jennings, R.J. Puddephatt, J. Organomet. Chem. 670 (2003) 27;
(g) S.K. Bhargava, F. Mohr, M.A. Bennett, L.L. Welling, A.C. Willis, Inorg. Chem. 40 (2001) 4271;
(h) S.K. Bhargava, F. Mohr, M.A. Bennett, L.L. Welling, A.C. Willis, Organometallics 19 (2000) 5628;
(i) M.A. Bennett, S.K. Bhargava, D.C.R. Hockless, L.L. Welling, A.C. Willis, J. Am. Chem. Soc. 118 (1996) 10469.

[8] V.W.-W. Yam, K.K.W. Lo, C.R. Wang, K.-K. Cheung, J. Phys. Chem. A 101 (1997) 4666.

[9] J.A. Miller, G. Zweifiel, Synthesis 2 (1983) 128.

[10] B.C. Berris, G.H. Hovakeemian, K.P.C. Vollhardt, Chem. Commun. (1983) 502.

[11] R. Eastmond, D.R.M. Walton, Tetrahedron 28 (1972) 4591.

[12] R. Wu, J.S. Schumm, D.L. Pearson, J.M. Tour, J. Org. Chem. 61 (1996) 6906.

[13] R. Rossi, A. Carpita, A. Lezzi, Tetrahedron 40 (1984) 2773.

[14] M.I. Bruce, B.K. Nicholson, O.B. Shawkataly, Inorg. Syn. 26 (1989) 324.

[15] D.D. Perrin, W.L.F. Armarego, Purification of Laboratory Chemical, 3rd ed., Pergamon, Oxford, 1988.

[16] P.T. Beurskens, G. Admiraal, G. Beurskens, W.P. Bosman, S. Garcia-Granda, R.O. Gould, J.M.M. Smits, C. Smykalla, The DIRDIF Program System, Technical Report of the Crystallography Laboratory, University of Nijmegen, The Netherlands, 1992.

[17] Crystal Structure Analysis Package, Molecular Structure Corporation, 1985 and 1982, The Woodlands, TX.

[18] C.M. Che, H.Y. Yip, W.C. Lo, S.M. Peng, Polyhedron 13 (1994) 887.

[19] R.J. Cross, M.F. Davidson, J. Chem. Soc. Dalton Trans. (1986) 411.

[20] V.W.-W. Yam, S.W.K Choi, J. Chem. Soc. Dalton Trans. (1996) 3411.

[21] (a) D. Li, X. Hong, C.M. Che, W.C. Lo, S.M. Peng, J. Chem. Soc. Dalton Trans. (1993) 2929.;
(b) M.J. Irwin, J.J. Vittal, R.J. Puddephatt, Organometallics 16 (1997) 5321.